J Mater Sci (2009) 44:556–562
DOI 10.1007/s10853-008-3070-7

Electron emission from La-Doped lead zirconate stannate titanate antiferroelectric ceramic under fast electric field pulses

Z. X. Sheng · Y. J. Feng · Z. Xu · X. L. Sun

Received: 4 April 2008 / Accepted: 17 October 2008 / Published online: 23 November 2008

Abstract High current density pulsed-electron emission is observed from a lead zirconate stannate titanate lanthanum-doped (PLZST) antiferroelectric ceramic disc on application of positive or negative triggering voltage pulses. Electron-emission pulse with a peak current density 1,400 A/cm^2 and a full-width at half-maximum (FWHM) duration of 560 ns was recorded in the presence of a 3.5 kV dc extraction voltage. It is higher than the various earlier results obtained using lead zirconate titanate ferroelectric ceramic. Self emission of electrons with a current density of 1.3 A/cm^2 and the FWHM duration of about 100 ns were also observed. Strong electrons emission was the co-effect of surface plasma and noncompensated charges at the surface of the antiferroelectric. Field-induced local phase transition in the vicinity close to triple junction results in primary electron emission from these areas. These primary emission electrons ignited surface plasma and then led to the strong emission.

Introduction

Electron emission from ferroelectric stimulated by fast switching has been studied for more than 40 years since Miller and Savage first discovered this phenomenon in 1960 [1]. In 1989, Gundel and co-workers at CERN reported an emission beam current density of more than 100 A/cm^2 by using lead zirconate titanate (PZT) and lanthanum-doped lead zirconate titanate (PLZT) as cathode materials [2]. Since then ferroelectric cathodes have been widely investigated by many groups all over the world. This is because the ferroelectric cathodes have special advantages when compared with traditional thermionic cathodes, such as room temperature operations, instant turn-on capabilities, and most importantly, high electron current emission [3–8].

Various applications have been built to utilize this intriguing phenomenon: flat panel displays, X-ray generation sources, infrared imaging sensors, gas spark switches, microwave tubes, and cathodes in lithography applications [8–14]. The electron emissions from these materials can be generated by different ways such as temperature variation, mechanical stress, light irradiation, and fast electric field pulses [7, 8]. Even though there has been a lot of work related to this phenomenon, complete understanding of the mechanism is still lacking [6–8]. This might indicate that their characteristics depend strongly on many factors such as sample parameters, experimental conditions, measurement methods, and so on.

Until now most high current densities are associated with PZT and PLZT ceramics [3–8]. Reported emission densities with other materials are relatively low. In studies by Peleg et al., it was shown that with $BaTiO_3$ it is possible to achieve formation of the plasma with density up to 10^{15} cm^{-3} using special form of the driving pulse [9].

In this article, a new experimental study of electron emission from antiferroelectric cathode material La-doped $Pb(Zr,Sn,Ti)O_3$ under application of negative triggering pulse is presented.

Experimental method

The PLSZT samples were made via conventional mixed-oxide processing. Reagent-grade raw materials, such as

Z. X. Sheng (✉) · Y. J. Feng · Z. Xu
Electronic Materials Research Laboratory, Xi'an Jiaotong University, Xi'an 710049, China
e-mail: shengzhxzhll@gmail.com

Z. X. Sheng · X. L. Sun
The Second Artillery Engineering Institute, Xi'an 710025, China

lead (II) oxide (PbO), titania (TiO_2), zirconia (ZrO_2), and lanthana (La_2O_3) were batched according to compositions. Excess PbO (2 mol.%) was used. The powders were ball milled for 5 h using ZrO_2 media, a polyethylene jar, and ethanol. The calcination temperatures were at 850 °C. Disks were cold-pressed, using a mixed binder of 8 wt% polyvinyl alcohol (PVA), and 3 wt% polyethylene glycol (PEG), and fired at 1,340 °C in a lead-rich atmosphere using a lead titanate ($PbTiO_3$) and lead zirconate ($PbZrO_3$) mixed source in a covered double crucible.

Each of the samples had a density of at least 98% of the theoretical density. After sintering, pellets (diameter of 18 mm) were polished to a thickness of 0.5 mm with 1200 grit SiC paper. After ultrasonic cleaning in water, samples were electroded with a grid pattern on one side and a full electrode (diameter of ~14 mm) on the opposite side. Figure 1a and b shows the rear electrode and front electrode of experimental samples. The width of silver electrode and bare ceramic in the grid pattern is 0.2 mm each, thereby the total exposed area on the surface of this sample was about 0.47 cm^2. A grid of silver electrodes (diameter of 12 mm) was patterned on the surface by screen printing, sintered at the temperature of 550 °C for 10 min, and the thickness of silver electrode was approximately 10 μm.

Figure 2 shows a schematic diagram of the experimental setup. Anti-ferroelectric (AFE) samples were placed into the vacuum chamber with the grid-electrode (GE) side facing the flat graphite electron collector (GC). The graphite collector area was at least 1.5 times larger than the emission area. The GE was kept at ground potential, while the driving pulse was coupled to the rear electrode. The distance between the sample and collector was set at 6 mm. A cable with an impedance of 50 Ohm was soldered on the electron collector and connected to the measurement circuit; the emission electrons were collected and flown through this 50-Ohm resistor. A two-channel digital real-time oscilloscope (Model TDS 460, Tektronix) with a 500-MHz bandwidth was used to measure the voltage drop across this AFE sample. A Pearson current monitor model 65/85 was use to measure the emitted current from the surface of AFE sample. A DC high-voltage generator can be connected and disconnected from the anode, see the detail in Fig. 2, so as to apply or not an external accelerating voltage through the diode gap. When no external accelerating voltage is applied through the gap, only the electrons acted upon by a repulsive force created at the surface are collected. The 0.1-μF capacitor inserted behind the anode, decouples it from ground for the application of external voltage, U_{ac}. That decoupling capacitor behaves as a short circuit for the short current pulses, thanks to the high value of its capacitance.

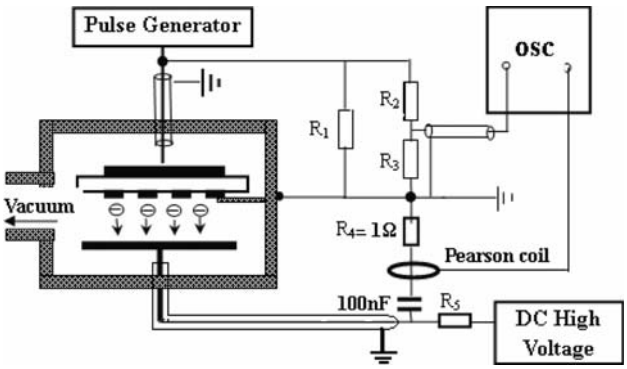

Fig. 2 Schematic diagram of the experimental setup

The pulse generator can generate a high-voltage (2.2 kV) unipolar pulse with a fast rise time ($t_{rise} = 1$ ns ± 30%/2 kV) and with duration of 500 ns. Impedance of the generator producing driving pulse is 50 Ohm. To minimize electrical noise, all connector cables were shielded and runs were made as short as possible. All studies were performed in a vacuum of 10^{-5} Torr and at room temperature.

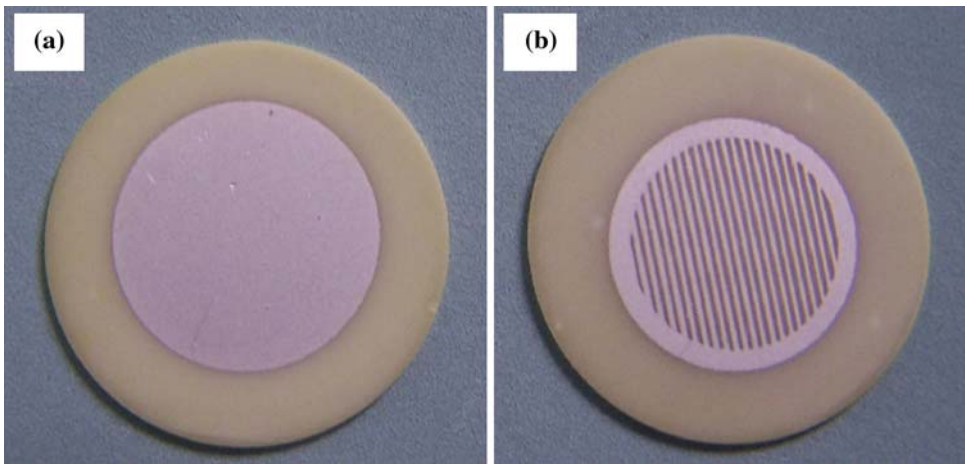

Fig. 1 Ferroelectric cathode samples **a** Rear electrode **b** Front electrode

Experimental results and discussion

In this experiment, we did our investigation with lead zirconate stannate titanate lanthanum-doped ceramics (PLZST) of composition $Pb_{0.94}La_{0.04}(Zr_{0.53}Sn_{0.30}Ti_{0.17})O_3$. The crystal with this composition is in antiferroelectric phase at room temperature.

Before electron-emission measurements, hysteresis loop characteristics of PLZST were measured at room temperature using improved Sawyer–Tower circuitry. Figure 3 shows the polarization of PLZST ceramics as a function of field. Figure 3 was obtained under application of a 1 Hz sine alternating voltage to the sample. Direct evidence of its antiferroelectricity can be observed in Fig. 3, which shows the typical double hysteresis loop. The maximal polarization (P_r) and forward electric switching field (E_c) of PLZST are of 29 μC/cm^2 and 2.8 kV/mm, respectively.

Current emission was successfully achieved upon application of fast electric field pulses to the rear electrode with a dc extraction voltage U_{ac} of 100 V. Two cases of positive and negative pulse excitations were considered. It was discovered that emission current occurred when triggering voltage reached 300–400 V, but electron emission was not reliable. The electron emission reliability increased with the increase of triggering voltage. Figure 4 shows the electron emission reliability under different triggering voltages. Defining the applied voltage threshold for ferroelectric emission as the voltage at which 80% or more of the applied voltage pulses result in current transport detected at the anode, we can find the threshold for emission from Fig. 4. For the sample of 0.5-mm thickness with Ag-coated emitting surface electrodes, the negative applied pulse threshold was approximately 500 V, and the positive pulse threshold was about 400 V. It would appear from this

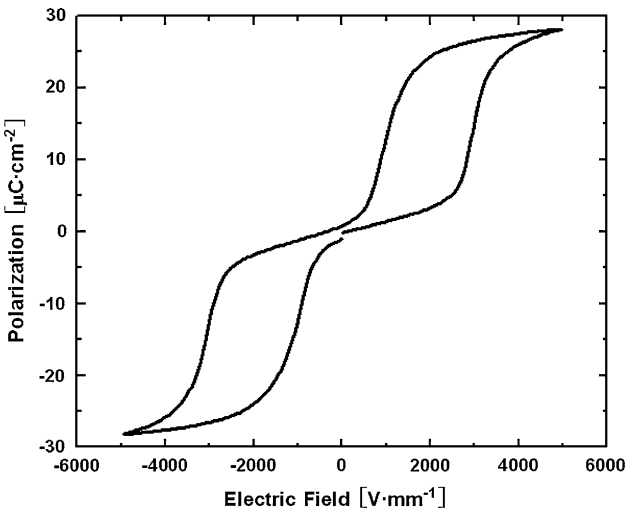

Fig. 3 Dependence of polarization on field

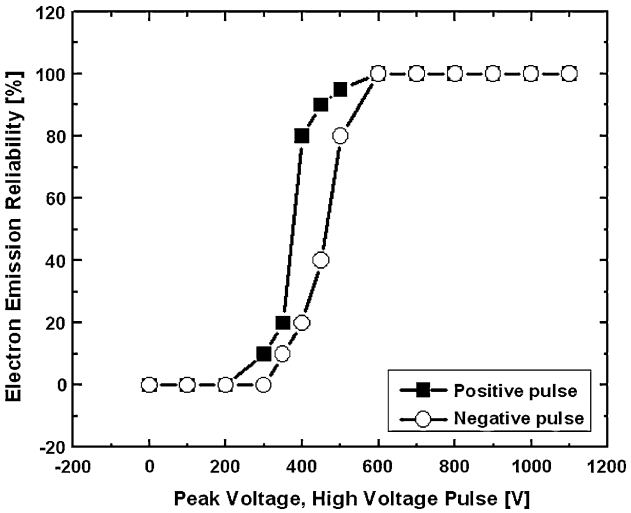

Fig. 4 Electron emission reliability as a function of applied unipolar pulse voltage. The emission threshold is arbitrarily defined as the peak applied voltage above which 80% or more of the applied voltage pulses result in current transport

data that positive applied pulses have a lower emission threshold voltage than that the negative applied pulses are.

It was found that no emission current occurred when the triggering voltage was below emission threshold voltage (300–400 V), and no emission current occurred when the PLZST cathode sample without the front electrode was triggered by the pulse voltage of 2 kV. These phenomena indicated that the measured current was not displacement current but emission current.

Figure 5a shows electron emission current of PLSZT ceramics as a function of dc extraction voltage for negative (or positive) triggering voltage of 600 V. The experimental results indicate that the emission current increases linearly with the increase of dc extraction voltage, and is independent of triggering voltage for higher dc extraction voltage. When the dc extraction voltage U_{ac} is 3.5 kV, the electron emission current reaches 690 A with a full-width at half-maximum (FWHM) duration of 560 ns, as shown in Fig. 5b. The corresponding emission current density reaches 1,460 A/cm^2. This emission current density is also larger than various earlier results obtained by using PZT or PLZT ceramic.

Figure 6a–d shows typical emission current waveform obtained with a negative triggering voltage of 600 V applied to the rear electrode of PLZST ceramics and an extraction potential of 60, 80, 100, and 120 V, respectively. One can see that there are always two distinguishable electron emission pulses per triggering voltage. The electrons were emitted at the field falling point as well as at the rising point. The first emission pulse (pulse 1) is a relatively stable emission pulse exhibiting only 30–40 ns delay time. The second emission pulse (pulse 2) always occurs

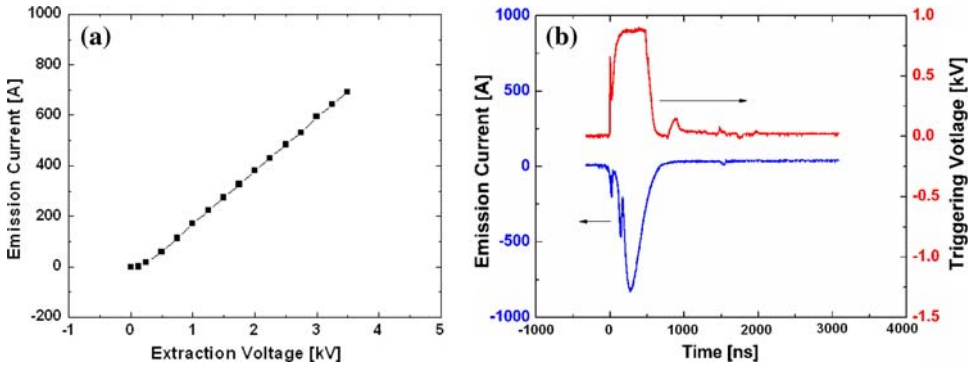

Fig. 5 **a** Emission current of PLSZT ceramics as a function of dc extraction voltage. **b** when the dc extraction voltage U_{ac} is 3.5 kV, the electron emission current reaches 690 A

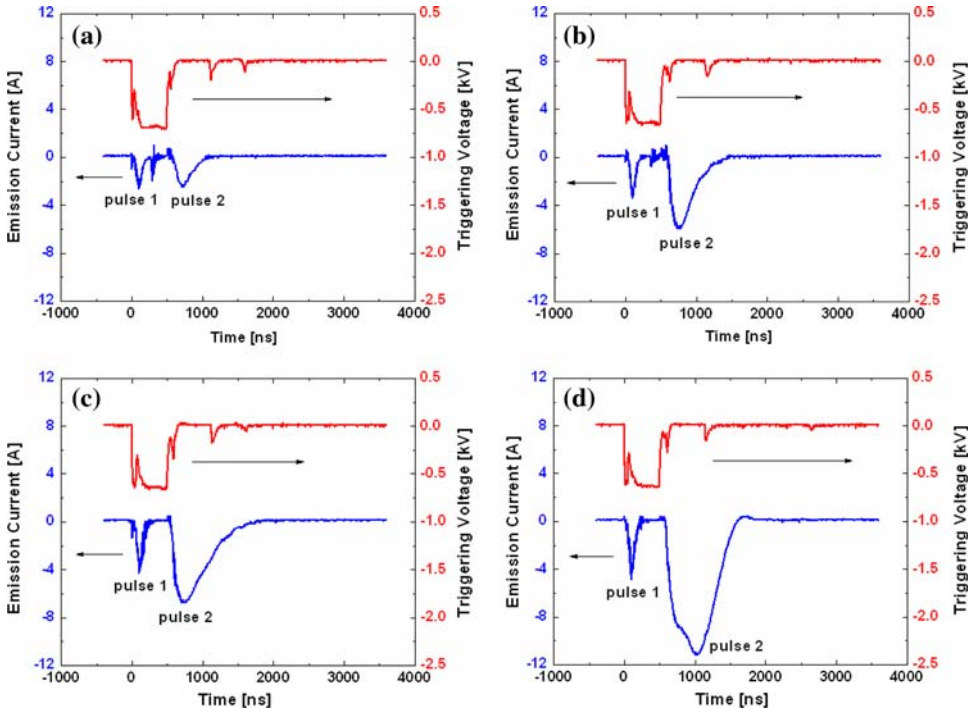

Fig. 6 Emission current waveform with a negative triggering voltage applied to the rear electrode of PLZST ceramics with different extraction potentials of **a** $U = 60$ V, **b** $U = 80$ V, **c** $U = 100$ V, and **d** $U = 120$ V

just after pulse 1. The second emission pulse occurs just at the end of triggering voltage pulse. Pulse 2 has higher amplitude and longer width than pulse 1. The position and amplitude of the two emission pulses are relatively steady. The pulse 1 increases from 2.5 A to 5 A with the increase of triggering voltage from 60 V to 120 V, and the FWHM duration of pulse 1 increases from 80 ns to 90 ns. The pulse 2 increases from 2.4 A to 11.2 A with the increase of extraction voltage from 60 V to 120 V, and the FWHM duration of pulse 2 increases from 250 ns to 700 ns. It would appear from this data that the pulse 2 showed a significant increase in amplitude and width with the increase of the extraction potential, while the pulse 1 showed almost no change.

Figure 7a–d shows typical emission current waveform obtained with a positive triggering voltage of 600 V applied to the rear electrode of PLZST ceramics and an extraction potential of 60, 80, 100, and 120 V, respectively. It is found that there are also two electron emission pulses per triggering voltage when dc extraction voltage $U_{ac} < 120$ V. For dc extraction voltage $U_{ac} > 120$ V, the two emission pulses merged, and a single electron emission current pulse with rather high amplitude and pulse width was observed. The amplitude of pulse 1 has a faster increase than that of pulse 2 with the increase of extraction potential.

Two quite different interpretations of strong electron emission from ferroelectric materials have been proposed presently [2, 4, 15–21]. Historically, the first one is based on specific properties of ferroelectric materials such as polarization reversal and various field-induced phase transitions, while the second one is ascribed to electron emission to surface plasma formation followed by electron extraction from the plasma.

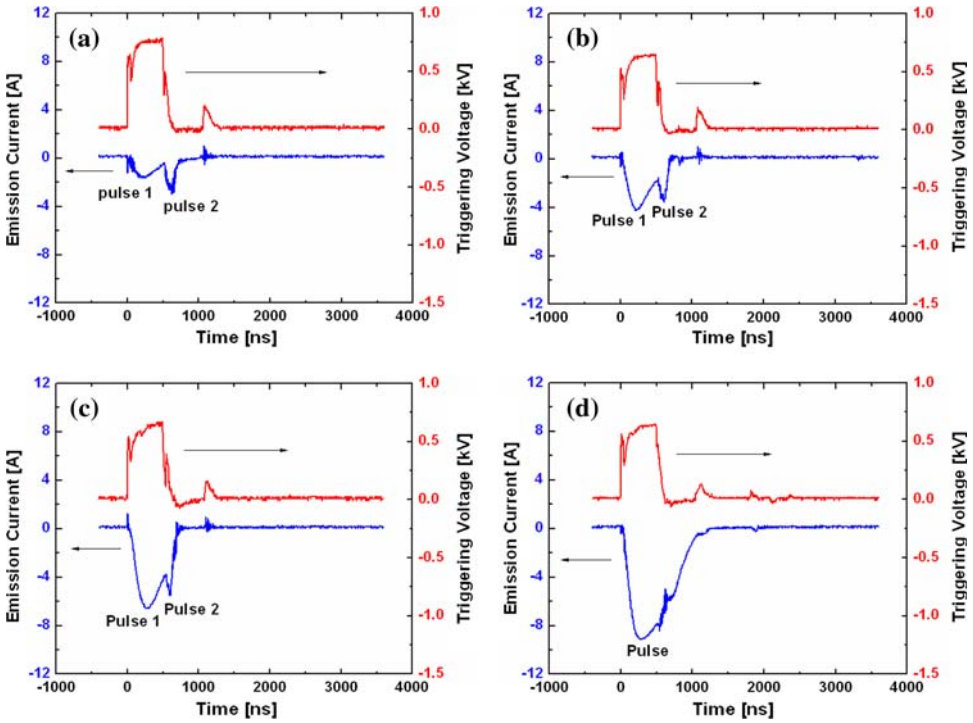

Fig. 7 Emission current waveform with a positive triggering voltage applied to the rear electrode of PLZST ceramics with different extraction potentials of **a** $U = 60$ V, **b** $U = 80$ V, **c** $U = 100$ V, and **d** $U = 120$ V

Strong electron emission from antiferroelectric ceramics has been already reported, and this phenomenon was ascribed to phase transition induced by strong pulse electric field. It is thought that if the electrons are emitted by the field-induced antiferro–ferroelectric phase transition, then there should be no emission current when the amplitude of triggering pulse is below the value of forward electric switching field in Fig. 3 (2.4 kV/mm). However, the experimental results show that an emission current of 3.5 A was observed when the triggering voltage was 0.4 kV, which is below the forward electric switching field, which was contradictory to the explanation of the phase transition of the antiferroelectrics.

In the triple junction region where metal, vacuum, and dielectric meet, the electric field can be roughly estimated as $E \approx \varepsilon_r U_0/\delta$ [3, 4, 22–24], where U_0, δ, and ε_r are the applied triggering voltage, dielectric thickness, and relative dielectric constant, respectively. As the average dielectric constant for PLZST in this experiment is about 700, and $U_0 = 600$ V, $\delta = 0.5$ mm, the enhancement of the electric field is 8.4×10^5 V/mm which is sufficient to induce local phase transitions in the vicinity close to the triple junction.

Figure 8 shows simulation of vector electric field distribution within and above the ferroelectric sample (performed by finite element program of ANSOFT MAXWELL10.0). One can see that in the ferroelectric surface between the grid electrodes, the field decreases with the increase of the distance from the grid electrode. However, the highest electric field was obtained in the triple point. This high electric field has the horizontal (parallel to the emitting surface of the sample) and vertical components. The horizontal component of the enhanced electric field may cause acceleration of priming electrons along the ferroelectric surface with subsequent electron avalanching and surface flashover. Consequently, surface plasma is generated.

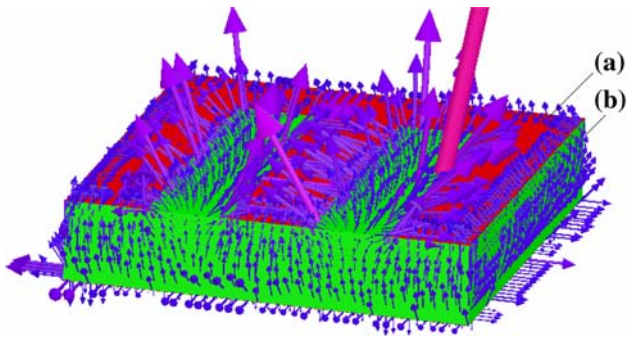

Fig. 8 Vector electric field distribution within and above the PLZST sample. (a) Silver electrode (b) PLZST ceramic

In addition to creating plasma on the ferroelectric surface, electric fields from the rear electrode accelerate the emissions of ions and electrons out of the plasma. Due to the plasma nature of the source of charged particles, we carried out experiments on ion beam generation. The generation of ion beams with current amplitude up to 16 A was demonstrated by a negative extraction potential of −150 V, as shown in Fig. 9.

More recently, there has been a trend toward believing that the single dipole in antiferroelectrics could be seen as a

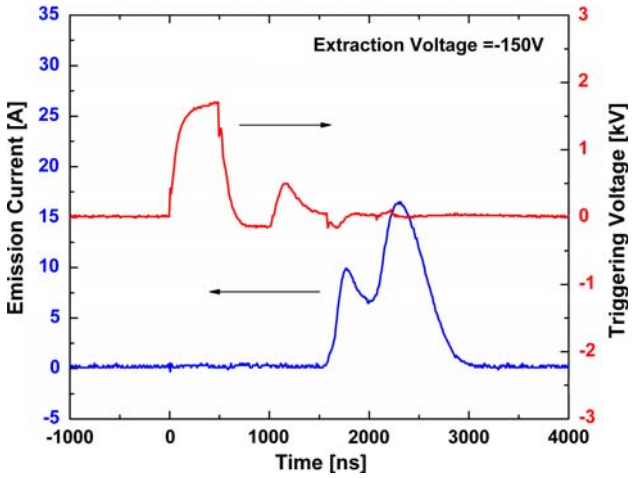

Fig. 9 Ion beams with current amplitude up to 16 A were obtained when a negative extraction potential of −150 V was applied to graphite collector

super-micro domain [25]. This condition permits very-rapid macroscopic polarization formation, because the very-fast sideways motion of these microdomain walls is possible without the need for a nucleation of new domains. In the case when a negative polarity pulse is applied to the rear electrode, the macroscopic polarization formation leads to the appearance of a noncompensated negative charge at the triple junction. The strong electrostatic field induced by noncompensated charges superimposes on the tangential components of the electric field induced by the diode voltage and forms a very strong field near the triple junction. Due to lowering of the potential barrier, a certain amount of electrons, tunneled out at the edge of the grid electrode. Then surface flashover will start at the triple junction, due to the initial release of emission electrons. Thus, the initial emission electrons and plasma electrons will be pulled out of the surface to form the pulse 1 with the FWHM duration of several tens of nanoseconds, as shown in Fig. 6a–d. This might be able to explain why strong electron emission occurs when the amplitude of triggering pulse is below the value of forward electric switching field. The exposed ceramic sample has almost the same potential as the rear electrode, which was below that of the grid electrode. The horizontal component of electric field on the exposed surface of ceramic sample may cause acceleration of priming electrons along the ferroelectric surface with subsequent electron avalanching and surface flashover. Plasma ions are attached to the surface to compensate bounded polarization charges. At the end of the triggering pulse, domain reversal leads to the appearance of noncompensated positive charge at the triple junction, which results in the formation of surface flashover plasma at the negative triple junction. Thus, plasma electrons are pulled out of the surface and can continue the process of surface plasma formation, which forms the second emission (pulse 2) with the FWHM duration of several hundreds of nanoseconds, as shown in Fig. 6a–d.

In the case when a positive polarity pulse is applied to the rear electrode, the situation is opposite. There is a more fast plasma expansion during the rise time when this plasma formation occurs which leads to large electron current (smaller gap). The abundant plasma electrons are pulled out of the surface to form pulse 1 with duration of several hundreds of nanoseconds. A certain amount of plasma electrons are attracted by the positive noncompensated charge of the domains. At the end of the triggering pulse, domain reversal, these electrons are ejected into the vacuum due to the accelerating field and repulsive force of the domain, which forms the sharp emission pulse 2, as shown in Fig. 7a–d.

Finally, let us consider the transformation of the electron emission waveform observed with the increase of extraction voltage. It was found from Fig. 6a–d that the pulse 2 showed a significant increase in amplitude and width with the increase of the extraction potential, while the pulse 1 showed a slight change. However, Fig. 7a–d shows a different situation from Fig. 6a–d. The surface plasma expansion velocity might be responsible for this phenomenon. In general, the application of the negative driving pulse leads to the formation of the plasma as well as in the case of the positive driving pulse. The difference between these two cases is as follows. In the case of the negative driving pulse, plasma ions are attached to the surface to compensate bounded polarization charges, and in the case of the positive driving pulse, plasma electrons are attached to the surface. Also, during the rise time when this plasma formation occurs, in both cases there is electron emission outward the ferroelectric surface. However, in the case of the positive driving pulse there is a more fast plasma expansion which results in pulse 1 (in Fig. 7) showing a significant increase in amplitude and width with the increase of the extraction potential. However, during the fall of the driving pulse, due to fast discharge, one obtains plasma formation and electron emission once more. There may be a more fast plasma expansion at the end of negative pulse which results in pulse 2 (Fig. 6) showing a significant increase in amplitude and width with the increase of the extraction potential.

Conclusion

In summary, strong electron emission can be successfully achieved with negative or positive polarity pulse applied to the rear electrode of PLZST antiferroelectric ceramic disc. The emission current waveforms obtained under negative polarity triggering voltage show different characteristics

from those observed under positive polarity triggering voltage. Enhancement of electric field and domain movement near the triple junction jointly leads to the primary emission electrons at the leading edge of triggering pulse; the horizontal component of electric field on the exposed surface of ceramic may promote the formation of surface flashover discharge during application of triggering pulse and the appearance of a noncompensated charge plays a very crucial role in the formation of the surface discharge plasma.

Acknowledgement This study was supported by the State Key Development Program for Basic Research of China (Grant No. 2002CB613307) and by the National Basic Research Program of China (Grant No. 50472052).

References

1. Miller RC, Savage A (1960) J Appl Phys 31(4):662
2. Gundel H, Reige H, Wilson EJN, Handerek J, Zioutas K (1989) Nucl Instrum Methods Phys Res A 280(1):1
3. Krasik YE, Chirko K, Dunaevsky A, Gleizer JZ, Krokhmal A, Sayapin A, Felsteiner J (2003) IEEE Trans Plasma Sci 31(1):49
4. Rosenman G, Shur D, Krasik YE, Dunaevsky A (2000) J Appl Phys 88:6109
5. Rosenman G, Shur D, Garb K, Cohen R, Krasik YE (1997) J Appl Phys 82(2):772
6. Riege H (1994) Nucl Instrum Methods Phys Res A 340:80
7. Fleddermann CB, Nation JA (1997) IEEE Trans Plasma Sci 25:212
8. Riege H, Boscolo I, Handerek J, Herleb U (1998) J Appl Phys 84:1602
9. Peleg O, Chirko K, Gurovich V, Felsteiner J, Krasik YE, Bernshtam V (2005) J Appl Phys 97:113307
10. Krasik YE, Chirko K, Gleizer JZ (2002) Eur Phys J D 19:89
11. Auciello OH, McGuire GE (1995-9-26) US Patent 5453661
12. Vollkommer F, Hitzschke L (2000-12-5) US Patent 6157145
13. Kovaleski SD (2005) IEEE Trans Plasma Sci 33(2):876
14. Kemp MA, Kovaleski SD (2006) J Appl Phys 100(11):1133061
15. Sampayan S, Caporaso G, Holmes C, Lauer EJ, Prosnitz D, Trimble DO, Westenskow GA (1994) Nucl Instrum Methods Phys Res A 340:90
16. Sampayan S, Caporaso G, Trimble D, Westenskow G (1995) IEEE Part Accel Conf 2:899
17. Jiang B, Kirkman G, Reinhardt N (1995) Appl Phys Lett 66(10):1196
18. Gundel H, Meineke A (1993) Ferroelectrics 146:29
19. Gundel H, Riege H, Wilson EJN, Handerek J, Zioutas K (1989) Ferroelectrics 100:1
20. Gundel H (1992) Integr Ferroelectr 2:207
21. Dunaevsky A, Krasik YE, Felsteiner J (2000) J Appl Phys 87:3270
22. Kofoid MJ (1960) AIEE Trans Part 3 79:991
23. Krasik Y, Dunaevsky A, Felsteiner J (1999) J Appl Phys 85:7946
24. Yong TK, Ki HY (2000) Appl Phys Lett 76:3977
25. Feng YJ, Xu Z, Wei YX, Yao X (2003) Acta Phys Sin 52(5):1256